AGU100 ADVANCING EARTH AND SPACE SCIENCE

Geophysical Research Letters

RESEARCH LETTER

10.1002/2017GL076808

Key Points:

- Each term in Poynting's theorem is calculated for an MMS-observed electron diffusion region (EDR)
- The equality of both sides of the equation shows that the terms are accurately determined
- Magnetic energy accumulation is observed at the electron current sheet around the X-point

Correspondence to:
K. J. Genestreti,
kevin.genestreti@oeaw.ac.at

Citation:
Genestreti, K. J., Cassak, P. A., Varsani, A., Burch, J. L., Nakamura, R., & Wang, S. (2018). Assessing the time dependence of reconnection with Poynting's theorem: MMS observations. *Geophysical Research Letters*, *45*. https://doi.org/10.1002/2017GL076808

Received 14 DEC 2017
Accepted 23 FEB 2018
Accepted article online 28 FEB 2018

Assessing the Time Dependence of Reconnection With Poynting's Theorem: MMS Observations

K. J. Genestreti[1], P. A. Cassak[2], A. Varsani[3], J. L. Burch[4], R. Nakamura[1], and S. Wang[5]

[1]Space Research Institute, Austrian Academy of Sciences, Graz, Austria, [2]Department of Physics and Astronomy, West Virginia University, Morgantown, WV, USA, [3]Mullard Space Science Laboratory, University College London, Dorking, UK, [4]Southwest Research Institute, San Antonio, TX, USA, [5]Astronomy Department, University of Maryland, College Park, MD, USA

Abstract We investigate the time dependence of electromagnetic-field-to-plasma energy conversion in the electron diffusion region of asymmetric magnetic reconnection. To do so, we consider the terms in Poynting's theorem. In a steady state there is a perfect balance between the divergence of the electromagnetic energy flux $\nabla \cdot \vec{S}$ and the conversion between electromagnetic field and particle energy $\vec{J} \cdot \vec{E}$. This energy balance is demonstrated with a particle-in-cell simulation of reconnection. We also evaluate each of the terms in Poynting's theorem during an observation of a magnetopause reconnection region by Magnetospheric Multiscale (MMS). We take the equivalence of both sides of Poynting's theorem as an indication that the errors associated with the approximation of each term with MMS data are small. We find that, for this event, balance between $\vec{J} \cdot \vec{E} = -\nabla \cdot \vec{S}$ is only achieved for a small fraction of the energy conversion region at/near the X-point. Magnetic energy was rapidly accumulating on either side of the current sheet at roughly 3 times the predicted energy conversion rate. Furthermore, we find that while $\vec{J} \cdot \vec{E} > 0$ and $\nabla \cdot \vec{S} < 0$ are observed, as is expected for reconnection, the energy accumulation is driven by the overcompensation for $\vec{J} \cdot \vec{E}$ by $-\nabla \cdot \vec{S} > \vec{J} \cdot \vec{E}$. We note that due to the assumptions necessary to do this calculation, the accurate evaluation of $\nabla \cdot \vec{S}$ may not be possible for every MMS-observed reconnection event; but, if possible, this is a simple approach to determine if reconnection is or is not in a steady state.

1. Introduction

Observations of magnetopause reconnection by Magnetospheric Multiscale (MMS) have revealed that energy conversion can occur in highly localized regions of the electron diffusion region (EDR) much more rapidly than previously expected (Burch & Phan, 2016; Burch et al., 2016; Chen et al., 2017; Ergun, Holmes, et al., 2016; Ergun et al., 2017; Genestreti et al., 2017; Hwang et al., 2017). This energy conversion rate is often expressed as the work rate of the nonideal electric field, or $\vec{J} \cdot (\vec{E} + \vec{v}_e \times \vec{B}) \equiv \vec{J} \cdot \vec{E}'$ (Zenitani et al., 2011), where $\vec{J}$ is the current density, $\vec{E}$ is the electric field, $\vec{B}$ is the magnetic field, and $\vec{v}_e$ is the electron bulk velocity. Cassak et al. (2017) analyzed 2.5-D particle-in-cell (PIC) simulations of three of these EDR events. They found that the MMS-observed energy conversion rates were up to several orders of magnitude larger than what was seen in their simulation for laminar steady state reconnection. One explanation offered by Cassak et al. (2017) is that the large-energy conversion rates observed by MMS may constitute localized bursts of activity in time and/or space rather than the global rate. Given the ubiquity with which larger-than-predicted $\vec{J} \cdot \vec{E}'$ are observed in magnetopause EDRs, it is possible that spatial and/or temporal burstiness is also ubiquitous.

To further investigate the steadiness or burstiness of energy conversion in the EDR, we consider Poynting's theorem, which in differential form is

$$-\frac{\partial u}{\partial t} = \nabla \cdot \vec{S} + \vec{J} \cdot \vec{E}, \tag{1}$$

where $u = (\epsilon_0 E^2 + B^2/\mu_0)/2$ is the electromagnetic energy density and $\vec{S} = \vec{E} \times \vec{B}/\mu_0$ is the Poynting vector. (Note that in Poynting's theorem, the energy conversion rate $\vec{J} \cdot \vec{E}$ contains both ideal $\vec{J} \cdot (-\vec{v}_e \times \vec{B})$ and non-ideal $\vec{J} \cdot \vec{E}'$ terms.) The rate of change of the electromagnetic energy density $\partial u/\partial t$ is zero in any perfectly steady state process, in which case the power exerted by the electric field on the particles $\vec{J} \cdot \vec{E}$ is balanced by the net electromagnetic energy flux into a volume $\nabla \cdot \vec{S}$ at every point in space. When integrated over a volume, Poynting's theorem says that the net electromagnetic energy flux into a volume is balanced

by the power exerted by the particles on the fields in the entire volume. For example, in an idealized (2-D, laminar, steady state and symmetric) reconnection ion diffusion region (IDR), the net difference between the electromagnetic energy densities flowing into the reconnection site $E_M B_L/\mu_0$ and expelled from the reconnection site $E_M B_N/\mu_0$ balances the rate of energy conversion within the reconnection site contributed mainly by $J_M E_M$. In this coordinate system, $\pm L$ is the direction of the reconnecting magnetic fields, N is the current sheet normal in the reconnection plane, and M completes the right-handed coordinate system. Swisdak et al. (2017) suggested that the dissipation of B_M may also occur within the asymmetric EDR, given the presence of a nonzero $J_N E_N$. With MMS, it is possible to approximate each of the terms in Poynting's theorem to assess the extent to which reconnection is steady state.

In this letter we present the first experimental determination of equation (1) in the context of reconnection (to our knowledge). To put our results in context, we also analyze the terms in Poynting's theorem in a 2.5-D PIC simulation of reconnection. Simulation results are discussed in section 2. In section 3 we describe our methodology for evaluating equation (1) from the MMS data, likely sources of errors, and results. Section 4 concludes with a discussion.

2. Poynting's Theorem From a 2.5-D PIC Simulation

We analyze the results of a fully kinetic PIC simulation that was carried out and analyzed in Cassak et al. (2017). The simulations and their setup are thoroughly discussed in that reference, so we only provide the most salient details here. The code in use is the P3D code (Zeiler et al., 2002). The initial setup of the simulation was chosen to match the upstream conditions of an asymmetric reconnection EDR event with an order 1 guide field observed by MMS on 8 December 2015 (Burch & Phan, 2016; Genestreti et al., 2017), which is not the same event as what is studied in section 3 but has a comparable out-of-plane (guide) magnetic field strength. The simulation was shown to reproduce some key features observed by MMS, for example, partially formed crescent-shaped electron distribution functions (Burch et al., 2016; Hesse et al., 2014, 2016) and a nonideal energy conversion rate that was peaked between the X and electron stagnation points.

The simulation was in two dimensions with doubly periodic boundary conditions in a rectangular domain of size 40.96×20.48 with a grid scale of 0.01 in units of d_{i0}, the ion inertial length with respect to a density of $n_0 = 15\ \mathrm{cm}^{-3}$. The reference magnetic field strength was 35 nT. The upstream values on the magnetosheath side were $B_L = 0.429, B_M = 0.4, n = 0.5, T_i = 1.313$, and $T_e = 0.123$; upstream values on the magnetospheric side were $B_L = 1, B_M = 0.357, n = 0.2, T_i = 1.361$, and $T_e = 0.271$. The full set of upstream parameters are listed in physical units and normalized values in Table 1 of Cassak et al. (2017), under the column header "8 Dec 2015." The electron mass is 100 times smaller than the ion mass and $c/c_{\mathrm{A0}} = 25$. The initial setup uses a double tanh profile for the magnetic fields and temperatures, with a density profile chosen to impose MHD force balance. There are initially an average of 500 particles per grid with equal weight. A small coherent perturbation is used to initiate reconnection. Lengths and times are presented in terms of reference values on the magnetosheath side, the inertial scale $d_{i,\mathrm{sh}}$, and the inverse ion cyclotron frequency $\Omega_{ci,\mathrm{sh}}^{-1}$, respectively.

We consider a time in the simulation, $\Omega_{\mathrm{ci,sh}} t = 17.16$ as shown in the vertical line in Figure 1a, where reconnection has evolved and is progressing at a more or less constant reconnection rate E, as shown as a function of time t. $\vec{J}\cdot\vec{E}\nabla\cdot\vec{S}$, and $\vec{J}\cdot\vec{E}+\nabla\cdot\vec{S}$ are shown in Figure 1b along a normal-directed cut through the X-point and also over a 2-D domain in Figures 1c–1e, respectively. To reduce the noise in the Poynting vector divergence term that always arises when taking derivatives of noisy data, we average the simulation results in time over $\sim 0.09\ \Omega_{\mathrm{ci,sh}}$ (10 time steps) and smooth the results in the spatial domain by $\sim 2\ d_{e,\mathrm{sh}}$ (or $\sim 0.2\ d_{i,e,\mathrm{sh}}$, which is 20 grid cells). Despite these efforts, fluctuations in $\nabla\cdot\vec{S}$ are observed with wavelengths near the smoothing length. However, these fluctuations are generally less than ~30% as large as the largest value of $\nabla\cdot\vec{S}$ at and very near the X-point, as seen in Figures 1b and 1c.

There is a strong $\vec{J}\cdot\vec{E} > 0$ in the center of the reconnection region (see Figures 1b and 1d). These data do not show noisy fluctuations because no derivatives needed to be taken to obtain $\vec{J}\cdot\vec{E}$. The strong positive $\vec{J}\cdot\vec{E}$ is colocated with a strong influx of electromagnetic energy, that is, $\nabla\cdot\vec{S} < 0$ (Figures 1b and 1c). These two terms balance one another to within the noise level of $\nabla\cdot\vec{S}$ (Figures 1b and 1e). This energy balance appears to be achieved beyond the center of the reconnection region as well, as $\vec{J}\cdot\vec{E} > 0$ and $\nabla\cdot\vec{S} < 0$ appear together in the magnetosheath-side ($N > 0$) separatrix of the northern ($L > 0$) reconnection region, and $\vec{J}\cdot\vec{E} < 0$ and $\nabla\cdot\vec{S} > 0$ appear together in the magnetosphere-side separatrix of the northern exhaust. This result is not unexpected for 2-D steady state laminar reconnection.

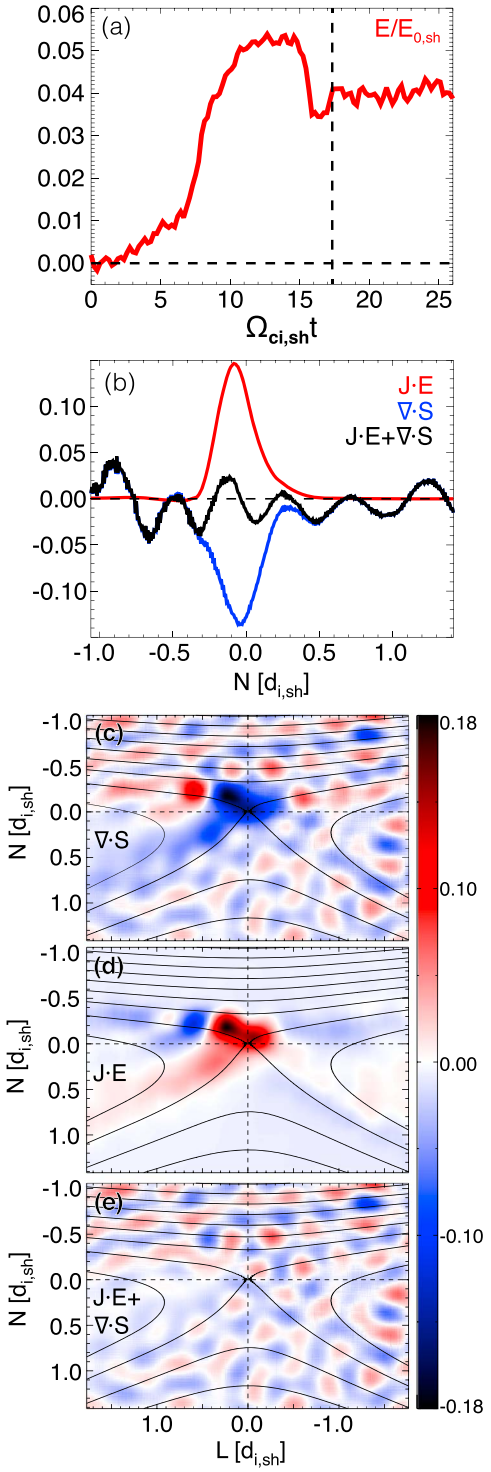

Figure 1. (a) The reconnection rate normalized to an electric field of 1.8 mV/m as a function of time normalized to $\Omega_{ci,sh}$, the inverse ion cyclotron frequency evaluated upstream in the magnetosheath. The vertical line shows the time where we calculate the quantities in (b)–(e). (b) The terms in Poynting's theorem evaluated along a normal-directed cut through the X-point. (c), (d), and (e): $\nabla \cdot \vec{S}$, $\vec{J} \cdot \vec{E}$, and $\nabla \cdot \vec{S} + \vec{J} \cdot \vec{E}$ (respectively) over the portion of the 2-D simulation domain surrounding the EDR. Length scales are normalized by $d_{i,sh}$, the asymptotic ion inertial length in the upstream magnetosheath. The solid black lines in (c)–(e) are contours of the magnetic flux function, that is, magnetic field lines.

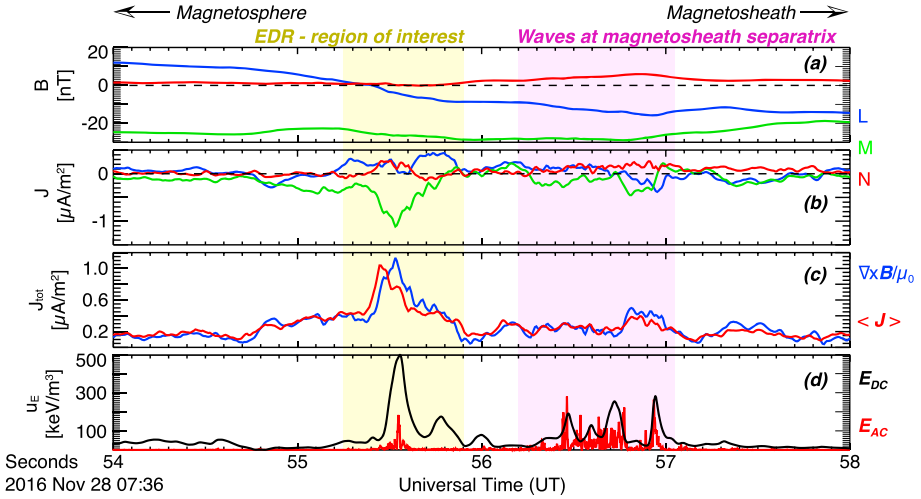

Figure 2. (a) Magnetic field vector and (b) current density vector in the LMN coordinate system defined for the X-point in Genestreti et al. (2018). (c) Total current density from the curlometer (blue) and averaged plasma moments (red). (d) The energy stored in the DC (low-frequency, black) and AC (high-frequency, red) portions of the electric field.

3. Poynting's Theorem From MMS Observations

On 28 November 2016, MMS crossed very slowly from the magnetosphere to the magnetosheath through an EDR (Genestreti et al., 2018). The separation between the MMS probes was close to the smallest separation used by MMS to date, at 6.4 km or ~4.5 $d_{e,\mathrm{sh}}$. When MMS crossed the magnetosphere-side separatrix, it was in the southern outer EDR or the IDR. MMS then moved northward into the central EDR, where nonideal energy conversion ($\vec{J} \cdot \vec{E}' > 0$) was observed near the X-point. Here all four spacecraft were simultaneously within the $\vec{J} \cdot \vec{E}' > 0$ region. Likely as a result of the slow crossing and small interprobe separation, Genestreti et al. (2018) found that the divergence and curl terms in the generalized Ohm's and Ampere's laws were very well resolved by the four-probe linear gradient technique (Chanteur, 1998). Furthermore, they found evidence that the structure of the current sheet and electric field may have been consistent with the 3-D and turbulent picture of asymmetric reconnection (Price et al., 2016, 2017), rather than the 2-D and laminar picture. They based this conclusion on observations of large in and out-of-the-reconnection plane electron pressure forces in the central EDR, as net pressure forces out-of-the reconnection plane cannot occur in the 2-D picture.

We use the highest time resolution data from MMS, including the DC magnetic field vector measured by the fluxgate magnetometers (Russell et al., 2016), the coupled AC-DC electric field vector from the electric field double probes (Ergun, Tucker, et al., 2016; Lindqvist et al., 2016), and the plasma electron moments from the fast plasma investigation (Pollock et al., 2016). We have to make a number of assumptions in order to approximate the terms in Poynting's theorem. (1) We assume that the fields and plasma moments vary linearly within the volume of the tetrahedron. (2) We smooth the AC-DC electric field data to obtain a DC field. We assume that $\nabla \cdot \vec{S}_{\mathrm{AC}}$ and $\partial u_{\mathrm{AC}}/\partial t$ (which cannot be resolved with the linear gradient technique) do not affect the balance of energy on the scale of the MMS tetrahedron.

First, we check the validity of these assumptions. Figure 2 shows MMS data near the intense out-of-plane electron current layer around the X-point. The region of intense current, nonideal energy conversion, electron agyrotropy, anisotropic electron heating, etc., is highlighted in yellow. The magnetosheath separatrix is in pink. As is shown in Figure 2c, the barycentric current density vector can be calculated nearly identically using either the curlometer technique (blue) or the four-spacecraft-averaged plasma moments data (red). This is an indication that the variation of the DC magnetic field may have been approximately linear within the tetrahedron volume. Genestreti et al. (2018) was also able to accurately calculate the electron pressure divergence term in generalized Ohm's law, which is an indication that the variations in the plasma electron moments were approximately linear. Figure 2d shows that the energy density of the AC electric field is small compared to the energy density in the DC field in the EDR. Here the DC field is determined by smoothing the coupled AC-DC electric field over 0.1 s and the AC field is defined as the difference of the two. Given that the speed of the magnetopause was estimated to be 31 km/s (Genestreti et al., 2018) and $d_{e,\mathrm{sh}} \approx 1.4$ km, this 0.1-s smoothing time corresponds to a distance of roughly 2 $d_{e,\mathrm{sh}}$, which is comparable to the spatial smoothing used

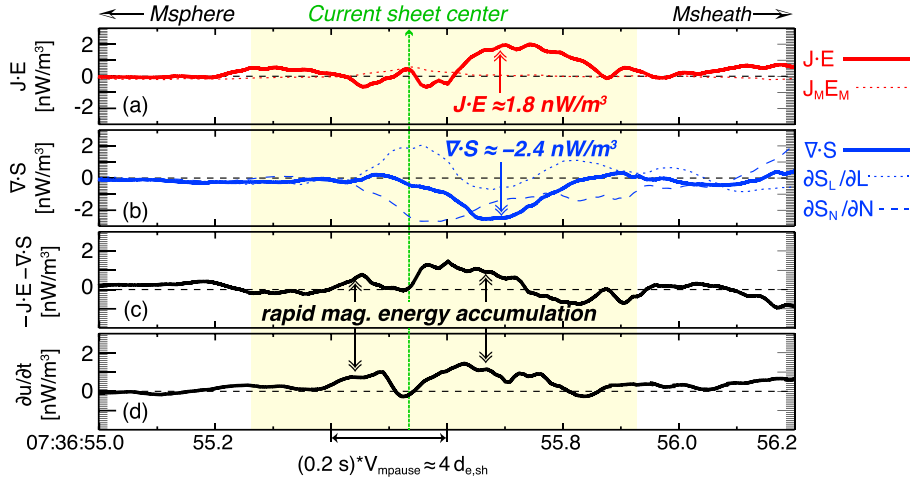

Figure 3. (a) The energy conversion rate $\vec{J} \cdot \vec{E}$ (solid line) and the rate of work of the reconnection electric field $J_M E_M$ (dotted). (b) The energy flux divergence $\nabla \cdot \vec{S}$ (solid) and the energy inflow rate $\partial S_N/\partial N$ (dashed) and outflow rate $\partial S_L/\partial L$ (dotted). (c) and (d) The per-volume rate of change of the electromagnetic energy density, as determined by the right- and left-hand sides of Poynting's theorem (equation (1), respectively.

to analyze our PIC simulation. As is shown in Figure 2d, the energy in the AC field only becomes comparable to the energy of the DC field in the separatrix (pink boxed) region. For this reason, we focus our investigation solely on the EDR.

We do not expect that the terms in equation (1) can be obtained for every MMS EDR event. In some cases, dissipation appears to be driven nearly entirely by high-frequency and intensely localized electric waves (Burch et al., 2018; Swisdak et al., 2017), such that the MMS tetrahedron may not resolve gradients over the associated scale sizes. In other cases, the spacecraft separation is larger than the size of the structure and the linear gradient technique cannot clearly and closely reproduce features of the reconnection region, for example, the dissipation rate (Genestreti et al., 2017; Torbert et al., 2016). As such, we define a "good quality" estimation of the terms in equation (1) as one in which both sides of the equation, which are determined separately, are roughly equivalent. That is, if $\partial u/\partial t$ and the errors associated with its calculation are roughly equal to $-\vec{J} \cdot \vec{E} - \nabla \cdot \vec{S}$ and their associated errors, then we assume that the error terms are small.

The terms in equation (1) are shown for the 28 November event in Figure 3. $\vec{J} \cdot \vec{E}$, shown in Figure 3a, is determined by the inner product of the curlometer current (Chanteur, 1998) and the four-point-averaged smoothed (DC) electric field in the X-line frame, where the X-line frame is determined by applying the spatiotemporal difference method (Shi et al., 2006) to the ~10-s time period surrounding the X-line crossing. (There are no major differences between the spacecraft frame and the X-line frame, however). $\nabla \cdot \vec{S}$, shown in Figure 3b, is determined by taking the linear divergence of the cross product of the DC electric and magnetic fields, also in the X-line frame. According to our quality criterion, $-\vec{J} \cdot \vec{E} - \nabla \cdot \vec{S}$ (Figure 3c) should be equivalent to our independently calculated $\partial u/\partial t$ (Figure 3d). Here $\partial u/\partial t$ is calculated as $\partial u/\partial t = \mathrm{d}u/\mathrm{d}t - \vec{v}_X \cdot \nabla u$, where the full time derivative is determined from the time series of the four-point-averaged DC fields and the X-line velocity $\vec{v}_X$ is used in the convective derivative. For all terms, r is approximated with the linear gradient technique (Chanteur, 1998).

First, we note that the left- (Figure 3d) and right-hand (Figure 3c) sides of equation (1) match extraordinarily well, which was our ultimate quality criterion. The largest value of $\vec{J} \cdot \vec{E} \approx 1.8$ nW/m^3 is dominated by the action of the in-plane electric field components E_L and E_N on the plasma. The largest energy conversion and influx rates are also observed at 7:36:55.7 UT between the reconnection midplane (7:36:55.5 UT) and the magnetosheath-side separatrix (7:36:56.4 UT), rather than at the center of the current sheet. Also, while $\vec{J} \cdot \vec{E}$ and $\nabla \cdot \vec{S}$ balance one another in the center of the current sheet, they are not balanced elsewhere. Both methods for calculating $\partial u/\partial t$ show that the electromagnetic energy density is increasing on either side of the current sheet. While the electric field intensity may also be changing in time, this energy density increase appears to be almost entirely from an increase in the magnetic energy density. The largest value of $\partial u/\partial t \approx 1.5$ nW/m^3 is comparable in magnitude to the largest value of $\vec{J} \cdot \vec{E} \approx 1.8$ nW/m^3 and is nearly 3 times larger

than the predicted value of $J_M E_{M,\mathrm{pred}} \approx 0.6$. Overall, we conclude that the EDR was not in a steady state at the time when and place where it was observed by MMS. Furthermore, we note that the cause of the energy accumulation is an overcompensation for the field-to-plasma energy conversion by more rapid energy influx (i.e., $-\nabla \cdot \vec{S} > \vec{J} \cdot \vec{E} > 0$).

Note that balance between $\vec{J} \cdot \vec{E}$ (Figure 3a) and $\nabla \cdot \vec{S}$ (Figure 3b) is achieved at the current sheet center near/at the X-line, which is marked by the vertical dashed green line in Figure 3. The energy conversion due to the reconnection electric field $J_M E_M$ (dashed red line in Figure 3a) is largest at the center of the current sheet. The value of $J_M E_M \approx 0.7$ nW/m^3 is also almost identical to the predicted maximum value for steady state reconnection with a reconnection rate of 0.1. Given the upstream conditions for this event listed in Table 1 of Genestreti et al. (2018) and the Cassak-Shay formula for the asymmetric reconnection rate (Cassak & Shay, 2007), the predicted reconnection electric field is $E_{M,\mathrm{pred}} \approx 0.5$ mV/m. Together with the observed maximum current density of $J_M \approx 1.1$ μA/m^2, this yields a predicted energy conversion rate of $J_M E_{M,\mathrm{pred}} \approx 0.6$ nW/m^3. Also, as expected, more electromagnetic energy enters the central current than is expelled from it, as $\partial S_N/\partial N \approx -2.4$ nW/m^3, $\partial S_L/\partial L \approx 1.9$ nW/m^3, and because of a small but finite $\partial S_M/\partial M$, we find $\nabla \cdot \vec{S} \approx -0.6$ nW/m^3. All of this leads to balance between the energy conversion and Poynting flux divergence terms at the X-point, where $-\vec{J} \cdot \vec{E} - \nabla \cdot \vec{S}$ and $\partial u/\partial t$ are both near zero. The balance of each of these terms matches qualitatively with both our simple theory and our PIC simulation results. However, since $\vec{J} \cdot \vec{E}$ is not balanced by $-\nabla \cdot \vec{S}$ elsewhere in the EDR, it is not clear if the balance of these two terms at/near the X-point is significant. (Note also that the exact agreement between $J_M E_M$ and $J_M E_{M,\mathrm{pred}}$ requires a reconnection rate of 0.1, which is only a canonical "order of magnitude" estimate rather than a known quantity.)

4. Discussion

We have investigated energy conversion in the central reconnection diffusion region by evaluating the source/loss ($\vec{J} \cdot \vec{E}$), flux divergence ($\nabla \cdot \vec{S}$) and time evolution ($\partial u/\partial t$) terms in Poynting's theorem. In theory, at the center of a symmetric steady state laminar 2-D reconnecting current sheet, the energy conversion rate $J_M E_M$ balances the energy flux divergence $\partial(E_M B_L/\mu_0)/\partial N + \partial(E_M B_N/\mu_0)/\partial L$ such that $\partial u/\partial t = 0$. We analyzed a 2.5-D PIC simulation of asymmetric reconnection and confirmed that during a period where the reconnection rate was steady state, energy balance ($\vec{J} \cdot \vec{E} = -\nabla \cdot \vec{S} \neq 0$ such that $\partial u/\partial t = 0$) is achieved in an area around the reconnection site in addition to the center of the reconnection site. For an MMS event, we found that the two sides of Poynting's theorem could be approximated uniquely and equivalently in such a way where the errors in each term were likely very small. Overall, we found that $\vec{J} \cdot \vec{E}$ and $\nabla \cdot \vec{S}$ did not balance one another as $-\nabla \cdot \vec{S} > \vec{J} \cdot \vec{E} > 0$, leading to magnetic energy accumulation in the EDR. However, at the center of a reconnecting current sheet at/near the X-line, MMS observed energy balance similar to our basic theory for steady state reconnection.

Our conclusion is that reconnection was not locally steady state at the time when and place where it was observed by MMS. Given the strength of $J_N E_N$ and the colocated negative value of $\partial S_L/\partial L$, we suggest that this MMS-observed EDR may be better described by the picture of spatially oscillatory dissipation of Swisdak et al. (2017). In their high-resolution 2.5-D and 3-D PIC simulations, Swisdak found that local fluctuations in the current sheet geometry can lead to the dissipation of the guide field B_M component. If B_M was being dissipated, then its strength would change with L and lead to $\partial S_L/\partial L < 0$, as was observed by MMS. This conclusion would be similar to that of Genestreti et al. (2018), which analyzed the same MMS event studied in this paper. Genestreti et al. found that the form of the generalized Ohm's law was not consistent with 2-D laminar and steady state reconnection.

Many open questions remain. Namely, can the observed energy imbalance be replicated with 2-D laminar time-dependent reconnection? Otherwise, are these observations better described by 3-D and/or turbulent reconnection? These open questions should be addressed in future simulation and theory-driven studies. We also do not know what influence high-frequency waves have on the energy balance equation. There were no very large amplitude waves observed for this event, but wave generation, dampening, and propagation should almost certainly have at least some small role in governing the energy balance. Finally, for this MMS event, is it significant that $\vec{J} \cdot \vec{E} = -\nabla \cdot \vec{S} \neq 0$ at the X-line but not on either side of the X-line, or is this a coincidence?

Acknowledgments
MMS data were obtained from the Science Data Center (SDC) at https://lasp.colorado.edu/mms/sdc/. The best calibrated level 3 electric field data are available upon request. K. J. Genestreti was funded by the FFG project 847969. P. A. Cassa k was funded by NASA grant NNX16AG76G and NSF grant AGS 1602769. Thanks to the entire MMS team that contributed to the success of the mission overall and the calibration of the instruments, without which this study would not have been possible. Thanks to N. Ahmadi, M. Akhavan-Tafti, P. Bourdin, L.-J. Chen, R.E. Ergun, S.A. Fuselier, R.B. Torbert, and M. Hesse for enlightening conversations and help with the MMS data. This event was identified during an International Space Science Institute (ISSI) meeting of the"MMS and Cluster observations of magnetic reconnection" group. The study made use of the Space Physics Environment Data Analysis Software (SPEDAS) package.

References

Burch, J. L., & Phan, T. D. (2016). Magnetic reconnection at the dayside magnetopause: Advances with MMS. *Geophysical Research Letters*, *43*, 8327–8338. https://doi.org/10.1002/2016GL069787

Burch, J. L., Torbert, R. B., Phan, T. D., Chen, L.-J., Moore, T. E., Ergun, R. E., et al. (2016). Electron-scale measurements of magnetic reconnection in space. *Science*, *352*(6290), aaf2939. https://doi.org/10.1126/science.aaf2939

Burch, J. L., Ergun, R. E., Cassak, P. A., Webster, J. M., Torbert, R. B., Giles, B. L., et al. (2018). Localized oscillatory energy conversion in magnetopause reconnection. *Geophysical Research Letters*, *45*, 1237–1245. https://doi.org/10.1002/2017GL076809

Cassak, P. A., & Shay, M. A. (2007). Scaling of asymmetric magnetic reconnection: General theory and collisional simulations. *Physics of Plasmas*, *14*(10), 102114. https://doi.org/10.1063/1.2795630

Cassak, P. A., Genestreti, K. J., Burch, J. L., Phan, T.-D., Shay, M. A., Swisdak, M., et al. (2017). The effect of a guide field on local energy conversion during asymmetric magnetic reconnection: Particle-in-cell simulations. *Journal of Geophysical Research: Space Physics*, *122*, 11,523–11,542. https://doi.org/10.1002/2017JA024555

Chanteur, G. (1998). Spatial interpolation for four spacecraft: Theory. In G. Paschmann & P. W. Daly (Eds.), *Analysis methods for multi-spacecraft data* (Chapter 14, pp. 349–368). Bern, Switzerland: International Space Science Institute.

Chen, L.-J., Hesse, M., Wang, S., Gershman, D., Ergun, R. E., Burch, J., et al. (2017). Electron diffusion region during magnetopause reconnection with an intermediate guide field: Magnetospheric multiscale observations. *Journal of Geophysical Research: Space Physics*, *122*, 5235–5246. https://doi.org/10.1002/2017JA024004

Ergun, R. E., Holmes, J. C., Goodrich, K. A., Wilder, F. D., Stawarz, J. E., Eriksson, S., et al. (2016). Magnetospheric Multiscale observations of large-amplitude, parallel, electrostatic waves associated with magnetic reconnection at the magnetopause. *Geophysical Research Letters*, *43*, 5626–5634. https://doi.org/10.1002/2016GL068992

Ergun, R. E., Tucker, S., Westfall, J., Goodrich, K. A., Malaspina, D. M., Summers, D., et al. (2016). The axial double probe and fields signal processing for the MMS mission. *Space Science Reviews*, *199*, 167–188. https://doi.org/10.1007/s11214-014-0115-x

Ergun, R. E., Chen, L.-J., Wilder, F. D., Ahmadi, N., Eriksson, S., Usanova, M. E., et al. (2017). Drift waves, intense parallel electric fields, and turbulence associated with asymmetric magnetic reconnection at the magnetopause. *Geophysical Research Letters*, *44*, 2978–2986. https://doi.org/10.1002/2016GL072493

Genestreti, K. J., Burch, J. L., Cassak, P. A., Torbert, R. B., Varsani, A., Ergun, R. E., et al. (2017). The effect of a guide field on local energy conversion during asymmetric magnetic reconnection: MMS observations, *122*, 11,342–11,353. https://doi.org/10.1004/2017JA024247

Genestreti, K. J., Varsani, A., Burch, J. L., Cassak, P. A., Torbert, R. B., Nakamura, R., et al. (2018). MMS observation of asymmetric reconnection supported by 3-D electron pressure divergence. *Journal of Geophysical Research: Space Physics*, *123*. https://doi.org/10.1002/2017JA025019

Hesse, M., Aunai, N., Sibeck, D., & Birn, J. (2014). On the electron diffusion region in planar, asymmetric, systems. *Geophysical Research Letters*, *41*, 8673–8680. https://doi.org/10.1002/2014GL061586

Hesse, M., Liu, Y.-H., Chen, L.-J., Bessho, N., Kuznetsova, M., Birn, J., & Burch, J. L. (2016). On the electron diffusion region in asymmetric reconnection with a guide magnetic field. *Geophysical Research Letters*, *43*, 2359–2364. https://doi.org/10.1002/2016GL068373

Hwang, K.-J., Sibeck, D. G., Choi, E., Chen, L.-J., Ergun, R. E., Khotyaintsev, Y., et al. (2017). Magnetospheric multiscale mission observations of the outer electron diffusion region. *Geophysical Research Letters*, *44*, 2049–2059. https://doi.org/10.1002/2017GL072830

Lindqvist, P.-A., Olsson, G., Torbert, R. B., King, B., Granoff, M., Rau, D., et al. (2016). The spin-plane double probe electric field instrument for MMS. *Space Science Reviews*, *199*, 137–165. https://doi.org/10.1007/s11214-014-0116-9

Pollock, C., Moore, T., Jacques, A., Burch, J., Gliese, U., Saito, Y., et al. (2016). Fast plasma investigation for magnetospheric multiscale. *Space Science Reviews*, *199*, 331–406. https://doi.org/10.1007/s11214-016-0245-4

Price, L., Swisdak, M., Drake, J. F., Cassak, P. A., Dahlin, J. T., & Ergun, R. E. (2016). The effects of turbulence on three-dimensional magnetic reconnection at the magnetopause. *Geophysical Research Letters*, *43*, 6020–6027. https://doi.org/10.1002/2016GL069578

Price, L., Swisdak, M., Drake, J. F., Burch, J. L., Cassak, P. A., & Ergun, R. E. (2017). Turbulence in three-dimensional simulations of magnetopause reconnection. *Journal of Geophysical Research: Space Physics*, *122*, 11,086–11,099. https://doi.org/10.1002/2017JA024227

Russell, C. T., Anderson, B. J., Baumjohann, W., Bromund, K. R., Dearborn, D., Fischer, D., et al. (2016). The magnetospheric multiscale magnetometers. *Space Science Reviews*, *199*, 189–256. https://doi.org/10.1007/s11214-014-0057-3

Shi, Q. Q., Shen, C., Dunlop, M. W., Pu, Z. Y., Zong, Q.-G., Liu, Z. X., et al. (2006). Motion of observed structures calculated from multi-point mag- netic field measurements: Application to Cluster. *Geophysical Research Letters*, *33*, L08109. https://doi.org/10.1029/2005GL025073

Swisdak, M., Drake, J. F., Price, L., Burch, J. L., Cassak, P. A., & Phan, T.-D. (2017). Localized and intense energy conversion in the diffusion region of asymmetric magnetic reconnection. *ArXiv:1710.04555*.

Torbert, R. B., Burch, J. L., Giles, B. L., Gershman, D., Pollock, C. J., Dorelli, J., et al. (2016). Estimates of terms in Ohm's law during an encounter with an electron diffusion region. *Geophysical Research Letters*, *43*, 5918–5925. https://doi.org/10.1002/2016GL069553

Zeiler, A., Biskamp, D., Drake, J. F., Rogers, B. N., Shay, M. A., & Scholer, M. (2002). Three-dimensional particle simulations of collisionless magnetic reconnection. *Journal of Geophysical Research*, *107*(A9), 1230. https://doi.org/10.1029/2001JA000287

Zenitani, S., Hesse, M., Klimas, A., & Kuznetsova, M. (2011). New measure of the dissipation region in collisionless magnetic reconnection. *Physical Review Letters*, *106*(19), 195003. https://doi.org/10.1103/PhysRevLett.106.195003